Energy Harvesting for Detecting Hidden Damages

Cian Flanagan
Postgraduate Student, School of Mechanical and Materials Engineering, University College Dublin, Dublin, Ireland

Vikram Pakrashi
Associate Professor, Director UCD Centre for Mechanics, Dynamical Sytems and Risk Laboratory, School of Mechanical and Materials Engineering, University College Dublin, Dublin, Ireland

ABSTRACT:

The paper presents how energy harvesting devices can be deployed to assess and estimate damages that are hidden to difficult to reach in terms of being able to provide instrumentation. To demonstrate this, the paper uses piezoelectric harvesters and analyses its open circuit dynamic response from different location of a damaged beam. This provides deflection and mode shape information. These responses are subsequently analysed via wavelets to identify damage location and extent. Subsequently, using prior modal and dynamic parameter information and knowledge, the paper uses a Bayesian statistical Identification Framework to determine the probabilities of crack location and extent within an obscured part of the structure or where the spatial modal shape or spatial wavelet is unavailable. The use of Recursive Bayesian Estimation can implement this framework as well. The paper demonstrates how novel sensors and materials can, with appropriate probabilistic techniques, provide better inspection and damage detection of our built infrastructure..

1. INTRODUCTION

Recent developments in energy harvesting technologies indicate that they have a potential to be a sensor for structural health monitoring (Cahill et al. 2016; Cahill et al. 2014). While such sensors have the potential to self-power there is still inadequate evidence of their potential applications and impact. In this regard, damage detection (Lee and Liew 2001; Lardies and Gouttebroze 2002) is important.

Damage detection using energy harvesting is dependent on the translation of kinematic responses due to damage to harvested energy, measured as voltage responses. Here, localization of damage is of particular interest. While closely spaced harvesters can give rise to damage localization, this is often not possible. An important challenge lies where damage is hidden or inaccessible. Modeshapes, strains or displacements may be unavailable, partially available or hidden from view. Here, there exists possibilities to estimate damage location and extent using recursive Bayesian estimates (Lam et al. 2005). This paper considers damage as an open crack in an Euler Bernoulli beam and demonstrates how vibration energy harvesters (VEH) can be adapted for such estimates to detect damage in hidden and inaccessible regions, where a sensor cannot be placed and visual inspection may not be possible.

2. PIEZOELECTRIC VEH

Piezo-VEH at the location of deployment coverts dynamic strain to energy via electromechanical coupling using (e.g. piezoceramics: lead zirconate titanate (PZT), polyvinylidene fluoride (PVDF)). For linear VEH, the energy conversion, this is (Erturk and Inman 2011) expressed as

$$\dot{U} = T_{ij}\dot{S}_{ij} + E_i\dot{D}_i \quad (1)$$

where U is the stored energy in piezoelectric continuum, T is the stress tensor, S is the strain tensor, E is the electric field tensor and D is the electric displacement tensor and overdot is time derivative. Equation 1 can be rearranged to obtain strain and electric displacement values as

$$S_p = s_{pq}^E T_q + d_{kp}E_k \quad (2)$$

$$D_i = d_{iq}T_q + \varepsilon_{ik}^T E_k \quad (3)$$

where s_{pq}^E is the elastic compliance matrix under a constant electric field E, d_{kp} is the piezoelectric constant matrix, D_i is the electric displacement vector and ε_{ik}^T is the permittivity under a constant stress T. The voltage response due to strain caused during vibrations can be obtained from equation 3 as $D_3 = \bar{e}_{31}S_1^{\tilde{p}} + \bar{\varepsilon}_{33}^S E_3$. The voltage response is

$$\frac{d}{dt}\left(\int_A \boldsymbol{D}.\boldsymbol{n}\, dA\right) = \frac{v(t)}{R_l} \quad (4)$$

resulting in time dependent voltage response as a function of mechanical strain as

$$C_{\tilde{p}}^{eq}\frac{dv(t)}{dt} + \frac{v(t)}{R_l} + \theta\int_0^L \frac{\partial^3 y_{rel}(x,t)}{\partial x^2 \partial t}dx = 0 \quad (5)$$

where $C_{\tilde{p}}^{eq}$ is the capacitance, $y_{rel}(x,t)$ is the deflection with respect to the static deflected shape, R_l is the external resistive load of an external circuit and θ is the electromechanical coupling coefficient. Strain is proportional to the curvature of Euler-Bernoulli beam, expressed as

$$S_l(x,z,t) = -z\,\frac{\partial^3 y_{rel}(x,t)}{\partial x^2} \quad (6)$$

where z is the distance from the neutral axis. Simplified this way, the voltage equation becomes

$$\frac{dv(t)}{dt} + \frac{v(t)}{\tau} = \frac{\bar{e}_{31}A}{C_{\tilde{p}}^{eq}}\,\frac{d}{dt}[S_1 + S_2] \quad (7)$$

The subscripts (1 and 2) on S indicate x and y directions respectively and $\tau = C_p R_l$ where capacitance $C_{\tilde{p}} = \frac{\bar{\varepsilon}_{33}^S bL}{z}$.

Patch-type piezoceramic VEH can be connected to a structure through adhesion and flexible PVDF is popular since it can respond easier to the dynamic strain of the host structure.

Cantilever type VEH with host structure vibrations as its base excitation and ability to tune to the natural frequency of the host to maximise output, are a common variant where both PZT and PVDF are popular. PZT typically is less flexible but comes with a advantage of slightly higher electromechanical coupling coefficient. Typically, metal cantilevers with outer layers covered with thin piezoceramic layer are used. The terms 'unimorph' and 'bimorph' refer to when one or both sides are covered with piezoceramic layers, respectively. Often, VEH are bimorphs. The electromechanical behaviour of PZT VEH is (Erturk and Inman 2011)

$$EI\frac{\partial^4 \bar{y}(x,t)}{\partial x^4} + c_s I\frac{\partial^5 \bar{y}(x,t)}{\partial x^4 \partial t} + c\frac{\partial \bar{y}(x,t)}{\partial t} + m\frac{\partial^2 \bar{y}(x,t)}{\partial t^2} - \theta v(t)\left[\frac{d\delta(x)}{dx} - \frac{d\delta(x-L)}{dx}\right] \quad (8)$$

and

$$C_{\bar{p}}^{eq}\frac{dv(t)}{dt} + \frac{v(t)}{R_l} + \theta\int_0^L \frac{\partial^3 \bar{y}(x,t)}{\partial x^2 \partial t}dx = 0 \quad (9)$$

The displacement $\bar{y}(x,t)$ is the deflection relative to the harvester's base, damping from air is represented by c and due to the material elasticity is $(c_s I)$. M_t is the tip mass at the free end and δ is the Dirac delta function. Following standard modal analysis,

$$\bar{y}(x,t) = \sum_{r=1}^{\infty}\phi_r(x)\eta_r(t) \quad (10)$$

where $\phi_r(x)$ is the mass-normalised r^{th} modeshape and $\eta_r(t)$ are r^{th} modal coordinates. The electromechanically coupled equations are

$$\frac{d^2\eta_r(t)}{dt^2} + 2\zeta_r\omega_r\frac{d\eta_r(t)}{dt} + \omega_r^2\,\eta_r(t) - \tilde{\theta}_r v(t) = f_r(t) \quad (11)$$

$$C_{\bar{p}}^{eq}\frac{dv(t)}{dt} + \frac{v(t)}{R_l} + \sum_{r=1}^{\infty}\tilde{\theta}_r\frac{d\eta_r(t)}{dt} = 0 \quad (12)$$

$$\widetilde{\theta_s} = \frac{\bar{e}_{31}w_h}{2h_{\bar{p}}}\left[\left(h_{\bar{p}} + \frac{h_{\bar{s}}}{2}\right)^2 - \frac{h_{\bar{s}}^2}{4}\right] \quad (13)$$

$$\tilde{\theta}_p = 2\tilde{\theta}_s \quad (14)$$

where $\tilde{\theta}$ is electromechanical coupling. Subscripts s and p denote series and parallel connections, respectively. For linear VEH, vibrations from first mode is dominant enough to ignore higher mode contributions. Parameters $h_{\bar{p}}$, $h_{\bar{s}}$ and w_h are the depth of the piezoceramic, substrate of the VEH and its width, respectively.

3. OPEN CRACK MODEL

A transverse open crack is considered causing local stiffness change. This is modelled as an equivalent rotational spring with stiffness

$K_T = \frac{M}{\theta_c}$ at crack location, where M and θ_c are the bending moment and slope, with $\theta_c = \int_0^{at} \frac{2}{E} K \frac{\partial K}{\partial M} dA$, respectively. The stress intensity factor (K) depends largely on the shape factor F which is a function of the crack-depth ratio (CDR), defined as the ratio between the depth of the crack (a) to that of the beam (h). Shape factors are empirically determined and for this paper

$$(a/h) = 1.22 - 1.40\left(\frac{a}{h}\right) + 7.33\left(\frac{a}{h}\right)^2 13.08\left(\frac{a}{h}\right)^3 + 14.0 \quad (15)$$

$$\theta_c = (72\pi M/Eth^2)F_1(a/h) \quad (16)$$

$$F_1\left(\frac{a}{h}\right) = 19.60\left(\frac{a}{h}\right)^{10} - 40.69\left(\frac{a}{h}\right)^9 + 47.04\left(\frac{a}{h}\right)^8 - 32.99\left(\frac{a}{h}\right)^7 + 20.29\left(\frac{a}{h}\right)^6 - 9.975\left(\frac{a}{h}\right)^5 + 4.602\left(\frac{a}{h}\right)^4 - 1.047\left(\frac{a}{h}\right)^3 \quad (17)$$

4. EULER BERNOULLI BEAM WITH AN OPEN CRACK MONITORED BY VEH

A simply-supported Euler-Bernoulli beam with rectangular cross section under forced vibrations is described by

$$EI\frac{\partial^4 y(x,t)}{\partial x^4} + c\frac{\partial y(x,t)}{\partial t} + m\frac{\partial^2 y(x,t)}{\partial t^2} = f(t) \quad (18)$$

where EI is the bending stiffness, m is mass per unit length, c is structural damping.

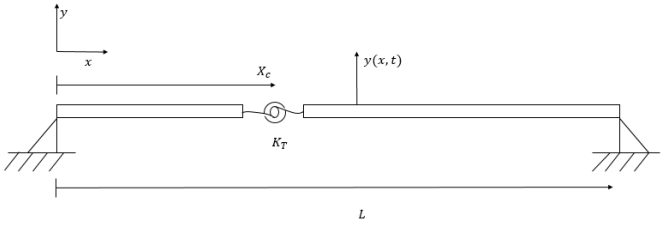

Figure 1: Euler Bernoulli beam with an open crack.

Method of separation of variables gives

$$y(x,t) = \sum_{r=1}^{\infty} \phi_r(x)\eta_r(t) \quad (19)$$

and substitution in Equation 18 results in

$$\frac{d^4\phi(x)}{dx^4} - \beta^4\phi(x) = 0 \quad (20)$$

$$\frac{d^2\eta(t)}{dt^2} + 2\zeta\omega_n\frac{d\eta(t)}{dt} + \omega_n^2 \quad (21)$$

where $\beta^4 = \omega_n^2\frac{m}{EI}$ and ω_n is the natural frequency. Modeshapes ($\phi(x)$) are expressed as

$$\phi(x) = A\sin\beta x + B\,cos\beta x + C\,sinh\beta x + D\,cosh\beta x \quad (22)$$

Coefficients A, B, C and D are determined from the boundary conditions of the beam supports and continuity conditions at crack location. To model the crack, two Euler-Bernoulli beams connected by a torsional spring is considered (Figure 1), on left (L) and right (R) with modeshapes

$$\phi_L(x) = A_2\sin\beta x + B_2\,cos\beta x + C_2\,sinh\beta x \quad (23)$$

$$\phi_R(x) = A_2\sin\beta x + B_2\,cos\beta x + C_2\,sinh\beta x \quad (24)$$

Boundary conditions at beam ends include displacement ($\phi_L(0) = \phi_R(L) = 0$) and moment ($\left.\frac{d^2\phi_L(x)}{dx^2}\right|_{x=0} = \left.\frac{\partial^2\phi_R(x)}{\partial x^2}\right|_{x=L} = 0$). Displacement continuity $\phi_L(a) = \phi_R(a)$, moment continuity $\phi_L''(a) = \phi_R''(a)$, shear continuity $\phi_L'''(a) = \phi_R'''(a)$ and slope compatibility $\Delta\phi_R''(a) = \phi_R'(a) - \phi_L'(a)$ at crack location lead to the solution of natural frequencies and modeshapes. Here, Δ is the non-dimensional crack flexibility parameter and a function of CDR. The boundary and compatibility conditions yield coefficients $A = \{A_1 B_1\ C_1\ D_1\ A_2\ B_2\ C_2\ D_2\}^T$ and matrix$M$ as $MA = 0$ where

$$\begin{bmatrix} \phi_L(0) \\ \phi_L''(0) \\ \phi_R(L) \\ \phi_R''(L) \\ \phi_L(a) - \phi_R(a) \\ \phi_L''(a) - \phi_R''(a) \\ \phi_L'''(a) - \phi_R'''(a) \\ \phi_R'(a) - \Delta\phi_R''(a) - \phi_L'(a) \end{bmatrix} \begin{Bmatrix} A_1 \\ B_1 \\ C_1 \\ D_1 \\ A_2 \\ B_2 \\ C_2 \\ D_2 \end{Bmatrix} = 0 \quad (25)$$

and M is

$$\begin{bmatrix} 0 & 1 & 0 & 1 & 0 & 0 & 0 & 0 \\ 0 & -1 & 0 & 1 & 0 & 0 & 0 & 0 \\ 0 & 0 & 0 & 0 & sin\beta L & 0 & sinh\beta L & 0 \\ 0 & 0 & 0 & 0 & -sin\beta L & 0 & sinh\beta L & 0 \\ siny & cosy & sinhy & coshy & -siny & -cosy & -sinhy & -coshy \\ -siny & -cosy & sinhy & coshy & siny & cosy & -sinhy & -coshy \\ -cosy & siny & coshy & sinhy & cosy & -siny & -coshy & -sinhy \\ cosy & -siny & -coshy & -sinhy & cos+\theta\beta siny & -siny+\theta\beta cosy & coshy-\theta\beta sinhy & sinhy-\theta\beta coshy \end{bmatrix} \quad (26)$$

Setting the determinant of this matrix to zero gives the characteristic equation (Sundermeyer, 1995)

$$[\sin(\beta Xc) + \alpha \sinh(\beta Xc)] = \frac{2K_t}{EI}\left[\frac{\sin(\beta Xc)}{\tan[\beta(L-Xc)]} + \cos(\beta Xc)\right] \quad (27)$$

where the constant α is

$$\alpha = \frac{\left(\left(\frac{\sin(\beta Xc)}{\tan[\beta(L-Xc)]}\right)+\cos(\beta Xc)\right)}{\left(\left(\frac{\sinh(\beta Xc)}{\tanh(\beta[L-Xc])}\right)+\cosh(\beta Xc)\right)} \quad (28)$$

and $\Delta = \frac{2K_t}{EI}$.

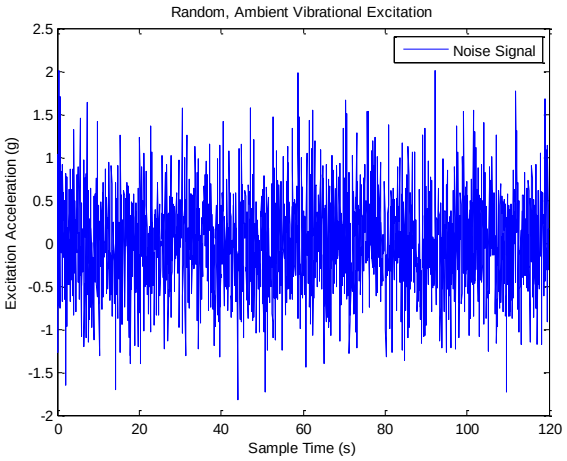

Figure 2: Gaussian white noise excitation on an Euler Bernoulli beam with an open crack fitted with VEH .

The modal coordinates are given by

$$\frac{d^2\eta(t)}{dt^2} + 2\zeta\omega_n\frac{d\eta(t)}{dt} + \omega_n^2\eta(t) = f(t) \quad (29)$$

and can be readily solved in state space form.

Beam excitation is considered by random ambient vibrations simulated as Gaussian white noise with zero mean (Figure 2).

To model energy harvesting based detection of damage, several VEH are considered to be discretely placed along the beam (Figure 3).

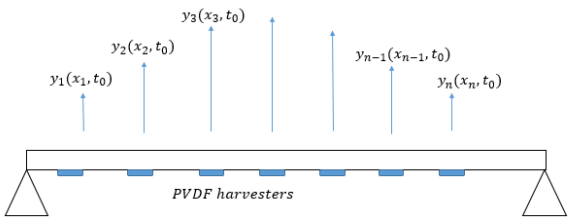

Figure 3: Patch VEH along placed the length of an Euler Bernoulli beam.

Comparing measured and estimated voltage from undamaged beam may provide damage information, as is often obtained using accelerometers (Ulriksen et al. 2016).

For a PVDF patch harvester placed x_n, the voltage response is

$$\frac{dv(t)}{dt} + \frac{v(t)}{\tau} = \frac{\bar{e}_{31}A}{C_{\tilde{p}}^{eq}}\left.\frac{dS}{dt}\right|_{(x_n,t_0)} \quad (30)$$

Cantilever type measurements can also be carried out this way (Figure 4).

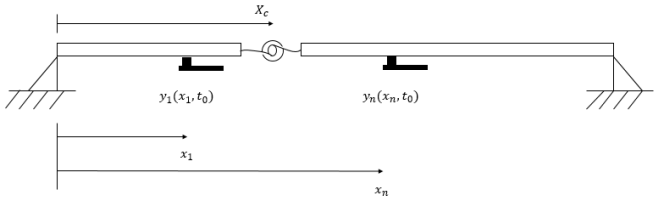

Figure 4: Cantilever VEH placed along the length of an Euler Bernoulli beam.

For these harvesters, the model can be expressed as

$$\{\dot{x}\} = [A]\{x\} + \{B\} \quad (31)$$

where $\{\dot{x}\}$ and $\{x\}$ are

$$\{x\} = \begin{Bmatrix} x_1 \\ x_2 \\ x_3 \end{Bmatrix} = \begin{Bmatrix} \bar{\eta}(t) \\ \frac{d\bar{\eta}(t)}{dt} \\ v(t) \end{Bmatrix} \quad (32)$$

$$\{\dot{x}\} = \begin{Bmatrix} \dot{x_1} \\ \dot{x_2} \\ \dot{x_3} \end{Bmatrix} = \begin{Bmatrix} \frac{d\bar{\eta}}{dt} \\ \frac{d^2\eta(t)}{dt^2} \\ \frac{dv(t)}{dt} \end{Bmatrix} \quad (33)$$

leading to

$$\begin{Bmatrix} \dot{x}_1 \\ \dot{x}_2 \\ \dot{x}_3 \end{Bmatrix} = \begin{bmatrix} x_2 \\ \bar{y} + \tilde{\theta}x_3 - \omega^2 x_1 - 2\zeta\omega x_2 \\ \frac{-x_3}{C_{\tilde{p}}^{eq}R_l} - \frac{\tilde{\theta}x_2}{C_{\tilde{p}}^{eq}} \end{bmatrix} \quad (34)$$

Following Erturk and Inman (2011)

$$\bar{y}(x,t)|_{t=0} = \kappa(x) \quad (35)$$

$$\left.\frac{\partial\bar{y}(x,t)}{\partial t}\right|_{t=0} = \mu(x) \quad (36)$$

Considering orthogonality of modes, including tip-mass (M_t) attached to the end of the harvester,

$$\eta(t)|_{t=0} = \int_0^L \kappa(x) m\phi(x)dx + \kappa(L)M_t\phi(L) + \vdash\left[\frac{d\kappa(x)}{dx} I_t \frac{d\phi(x)}{dx}\right]_{x=L} \quad (37)$$

$$\left.\frac{d\eta(t)}{dt}\right|_{t=0} = \int_0^L \mu(x) m\phi(x)dx + \mu(L)M_t\phi(L) + \left[\frac{d\mu(x)}{dx} I_t \frac{d\phi(x)}{dx}\right]_{x=L} \quad (38)$$

$$v(0) = v_0 \quad (39)$$

An initial base voltage of zero considered and

$$\begin{bmatrix} \eta(0) = 0 \\ \eta'(0) = 0 \\ v_0 = 0 \end{bmatrix} \quad (40)$$

5. A RECURSIVE BAYESIAN ESTIMATION APPROACH

The presence of damage is now considered to be hidden or inaccessible as indicated in Figure 5.

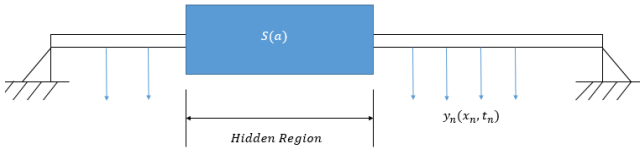

Figure 5: Hidden or inaccessible damage on an Euler Bernoulli beam.

A Bayesian approach is considered in this regard to estimate the presence, location and extent of such damage using energy harvesting signatures.

5.1. A Bayesian Approach for Detecting Hidden or Inaccessible Damage

5.1.1. Bayesian Inference and Statistical Identification

Bayes' theorem states

$$p(\theta|\boldsymbol{x}) = \frac{p(\boldsymbol{x}|\theta)p(\theta)}{p(\boldsymbol{x})} \quad (41)$$

where θ is the hypothesis, $\boldsymbol{x} = x_1, x_2, .. x_n$ is the measured or observed data, $p(\theta|\boldsymbol{x})$ is the posterior - the probability of the hypothesis given the observed data. The likelihood $p(\boldsymbol{x}|\theta)$ is the probability of observing data given the hypothesis and the prior $p(\theta)$ is the belief concerning the hypothesis. To make the likelihood a probability distribution, it is normalised by $p(\boldsymbol{x})$ as

$$p(\boldsymbol{x}) = \int_{S(\theta)} p(\boldsymbol{x}|\theta)p(\theta)d\theta = c \quad (42)$$

where $S(\theta)$ refers to the state-space occupied by hypothesis and c is the normalising constant. Since it is almost impossible in practice to measure or compute it, this issue is avoided by constraining the probability within a state-space to a range of possible values that the parameter or hypothesis may take. Combined with likelihood probability, which can be integrated and dividing each point within the state-space by the integral the normalizing constant is approximated and a normalized distribution curve is obtained. The choice of prior and its characteristics thus influences results and bias in it can lead to inaccuracy and convergence challenges.

For dynamical systems and parameters, there are methods to evaluate uncertainties in structural and crack parameters via Bayesian Statistical Identification Framework (Katafygiotis and Beck 1998; Lam et al. 2005). The approach relies on the fact that there exists some optimal variance (Lam et al. 2005) for all of the parameters in question concerning crack/damage parameters as well as structural parameters. It is defined as

$$J(a) = \frac{1}{NN_N}\sum_{n=1}^{N} \|\mathcal{I}[p(n)] - \mathcal{I}[q(n;\boldsymbol{a})]\|^2 = \hat{\sigma}^2 \quad (43)$$

where $\mathcal{I}(v)$ is the imaginary part of the vector v. Note, the imaginary part is selected harmonic wavelets are used for crack detection and they are complex. The vector $p(n)$ is the spatial wavelet transform of measured deflection curve at the n^{th} time step and $q(n)$ is the vector containing the spatial wavelet transform of the calculated deflections obtained from the known fundamental modeshape, based on the model for some given parameters $\boldsymbol{a}$. The constants N_N and N are the number of observed measurements and time-steps respectively. The parameter $\hat{\sigma}^2(a)$ represents the optimal variance in the predictions error model for given crack and structural parameters $\boldsymbol{a}$ and from which a probability distribution can be calculated for the likelihood.

This is true for large numbers of N and increasing the number of sampling points will improve the accuracy of the analysis. For measurement, this would mean that more energy harvesters would lead to increase in accuracy due to increase in information to carry out relevant statistical analyses.

5.1.2. Recursive Bayesian Estimation and Bayesian Filtering

Presence of noise can mask useful features of interest in measurement. An iterative Bayesian algorithm can seek the most probable values of uncertain parameters, addressing presence of noise. Consider a length along the beam to be obscured or hidden region containing the open crack (Figure 5). Measurements outside this length is possible. For the crack location, the range of its existence is the hidden length along the beam. The crack extent is also limited by its CDR range and a maximum of 0.5 is considered. The assumption is that there exists a point of optimal variance which is true for all uncertain parameters within the model. This is determined by the difference between the measured spatial wavelet of the energy harvesting signal and the calculated signal.

$$\hat{\sigma}^2 = \frac{1}{N}\sum_{i=1}^{N}(\boldsymbol{x_i} - \bar{x})^2 \quad (44)$$

where $\boldsymbol{x_i}$ is the spatial wavelet transform of measurements taken from the system, $\bar{x}$ is the calculated response and N is the number of measurements taken. For wavelet analysis, this is treated as the number of points selected for measurement or the length of the measurement vector. So, this can be the number of harvesters or points along the structure which are monitored.

A uniform prior $p(\theta) = \frac{1}{N_s}$ is chosen here due to uncertainty in system. Measurement is a linear combination of noise and the true signal as

$$x = \theta + \eta \quad (45)$$

With the assumption that the true signal (θ) is Gaussian, the measurement is also distributed similarly. The noise is assumed to be Gaussian with mean 0 and variance σ^2. The measurement mean is

$$E[\boldsymbol{x}] = E[\theta] + E[\eta] \quad (46)$$

where $E[x]$ is the expectation. Since noise has a 0 mean,

$$E[\boldsymbol{x}] = E[\theta] \quad (47)$$

Consequently, measurements have a distribution of $\mathcal{N}(\theta, \sigma^2)$. Since the goal is to estimate two values which share the same optimal variance (crack location and crack extent) a matrix is required as $\Sigma = \begin{bmatrix} \hat{\sigma}^2 & 0 \\ 0 & \hat{\sigma}^2 \end{bmatrix}$. A likelihood of a multivariate normal distribution can the be approximated as

$$p(x|\theta) \approx \frac{1}{\sqrt{2\pi^k \Sigma}} \exp\left[-\frac{1}{2}(\boldsymbol{x_i} - \mu)^T \Sigma^{-1}(\boldsymbol{x_i} - \mu)\right] \quad (48)$$

The subscripts are the indexing of measurement data points. Due to the availability of the optimal variance $\hat{\sigma}$, the standard deviation can be used to generate random points with such standard deviation within the state space. These points can be treated as noise about the true value representing the uncertain parameters. A total of k points are considered for the proposed algorithm where

$$p(\theta|x)_k = \frac{p(x|\theta)_k p(\theta)_k}{p(x)_k} \quad (49)$$

$$p(\theta)_{k+1} = p(\theta|x)_k \quad (50)$$

Iteration at each stage computes a new likelihood for each dataset or noise point. This is then combined with the prior and as a product, normalised. With this data, the posterior PDF can be obtained and the resulting point or state of maximum probability. This probability state is then brought back into the algorithm as the new prior; which then combined with a newly calculated likelihood based on next data point x_{k+1}. The point at which this new prior is at its maximum probability becomes the new mean. This process is repeated until there is insignificant difference between iterations, and lower than a pre-selected threshold or until a desired number of iterations are complete. The coordinates of the state of maximum probability are the estimated parameter values: the crack location within the hidden region and the extent of the crack, from which the CDR can be found.

5.2. Results

5.2.1. Simulation Parameters

A 10m long beam, with 30GPa Young's modulus with rectangular cross-section (0.25m width x 0.5m depth) is considered with 2nd moment of area about the neutral axis as 0.026 m^4, mass density 2400 kg/m^3 and 1% damping ratio. The open crack is at a distance $X_c = 4.3$m from the left support, with a nominal crack-depth ratio of 0.1 and the crack extent Δ being 37.7264. The properties of PZT-5H, popular for cantilever bimorphs is considered with piezoelectric constant $\bar{e}_{31}$ =16.6 C/m^2, density of 7750 kg/m^3, compliance $\bar{c}$ = 60.6 MPa and permittivity $\varepsilon_{33}^{S} = 13.3$ nF/m. For PVDF, a capacitance (C) of 95 nF and a resistive load R_l of 100 Ω is considered, with piezoelectric constant $e_{31} = 8.55$ C/m^2.

5.2.2. Modal Analysis: Damaged and Undamaged

Natural frequencies and modeshapes of the damaged and undamaged beams were computed and the small variation between the two is presented in terms of curvature in Figure 6. Even for a damage sensitive parameter like curvature, the changes are small, and prone to noise masking.

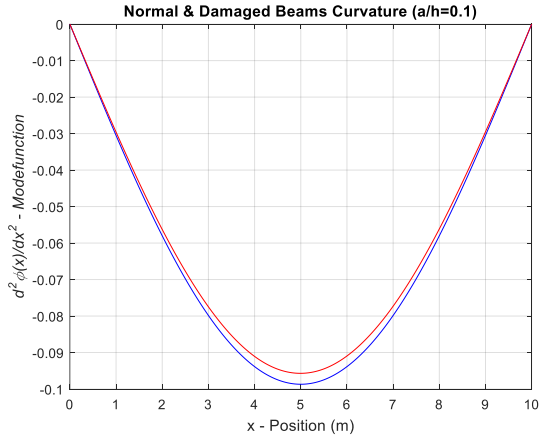

Figure 6: Damaged (CDR=0.1) and undamaged beam curvature

PVDF harvesting voltage is proportional to the strain of the host surface, assuming perfect contact and low thickness of these patches. Strain, is proportional to curvature, which is approximated as the 2nd spatial derivative of the first mode. For hidden damages to be detected from harvested voltage, the challenge can then reduce to the detection of the location of a certain magnitude of a function equal to (or of the order of) what is detected by wavelet analysis (Figure 7), in the presence of noise. The accuracy of estimating the magnitude will be a function of the extent of noise, the size of the magnitude, the location and the extent of hidden or inaccessible length.

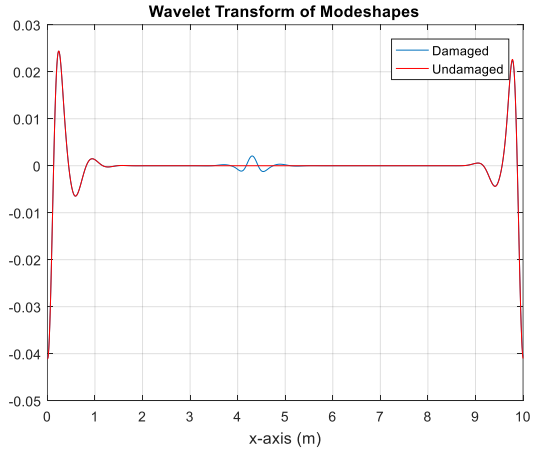

Figure 7: Damaged detection for CDR=0.1 using continuous wavelet transform.

5.2.3. Bayesian Estimation of Hidden Damage

The Bayesian algorithm proposed in this paper was implemented to find the location and extent of the hidden damage. Here, a location of (3,5) is affected by noise, which has a variance of 4. Initially, there is uncertainty around location of the true value. The initial uniform prior is iterated until a converged estimate is obtained (Figure 8).

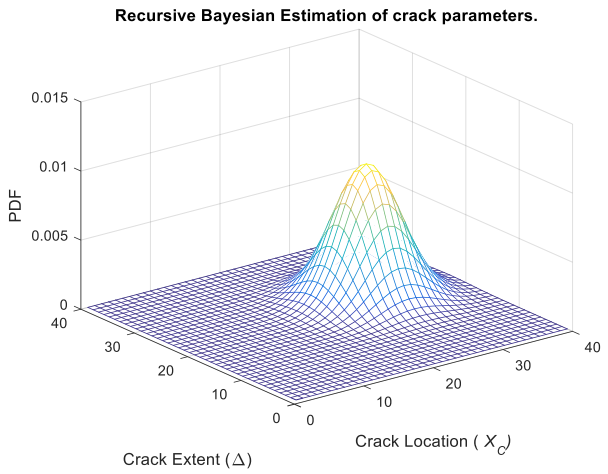

Figure 8: Detection of hidden damage location and extent using recursive Bayesian estimation

6. CONCLUSIONS

Energy harvesting devices can be effective measuring instruments, particularly in the domains where ambient sources of noise are involved. It can be seen that PVDF based devices can effectively directly measure the local strains of a host structure and consequently, determine if any damage is present based on the amount of output energy or voltage they produce. A system of such measuring devices configured correctly could provide information of the host structures related to fundamental modal responses. This combined with analyses techniques such as wavelets can prove effective at detecting damage despite the presence of noise. Implementation of Bayesian statistical estimation proves effective in tackling hidden damage or damages that are partially obstructed or are in difficult locations to access. This ability to be able to assess hidden or partially obstructed damaged increase and improve the abilities of such devices to move to a self-powered paradigm, while allowing for use of less number of sensors.

7. ACKNOWLEDGEMENTS

The authors would like to acknowledge Science Foundation Ireland funded NexSys (21/SPP/3756) project, Sustainable Energy Authority of Ireland funded REMOTEWIND RDD/613 project.

8. REFERENCES

Cahill, P, Jaksic V, Keane J, O'Sullivan A, Mathewson A, Ali SF, and Pakrashi V. (2016). Effect of Road Surface, Vehicle, and Device Characteristics on Energy Harvesting from Bridge Vehicle Interactions. *Computer-Aided Civil and Infrastructure Engineering*, 31 (12): 921–35.

Cahill, P, Ni Nuallain NA, Jackson N, Mathewson, A., Karoumi R and Pakrashi V. (2014). Energy Harvesting from Train-Induced Response in Bridges. *Journal of Bridge Engineering*, 19 (9): 1–11.

Erturk, A, and Inman., D.J. (2011). Piezoelectric Energy Harvesting. Piezoelectric Energy Harvesting. doi: 10.1002/9781119991151.

Katafygiotis, L.S., and Beck. J.L. (1998). Updating models and their uncertainties in model identifiability. *Journal of Engineering Mechanics* 124(4), 463–67.

Lam, H. F., Y. Y. Lee, H. Y. Sun, G. F. Cheng, and X. Guo. (2005). Application of the Spatial Wavelet Transform and Bayesian Approach to the Crack Detection of a Partially Obstructed Beam. *Thin-Walled Structures*, 43 (1): 1–21.

Lardies, Joseph, and Stéphane Gouttebroze. 2002. Identification of Modal Parameters Using the Wavelet Transform. *International Journal of Mechanical Sciences*, 44(11): 2263–83.

Lee, Y. Y., and K. M. Liew. (2001). Detection of Damage Locations in a Beam Using the Wavelet Analysis. *International Journal of Structural Stability and Dynamics*, 1(3): 455–65.

Mallat, Stéphane. (1999). A Wavelet Tour of Signal Processing. A Wavelet Tour of Signal Processing, doi:10.1016/B978-012466606-1/50004-0.

Sundermeyer, J.N., and Weaver, R.L. (1995). On crack identification and characterization in a beam by non-linear vibration analysis. *Journal of Sound and Vibration*,183(5), 857–871.

Ulriksen, M. D., Tcherniak, D., Kirkegaard, P.H., and Damkilde, L. (2016). Operational Modal Analysis and Wavelet Transformation for Damage Identification in Wind Turbine Blades. *Structural Health Monitoring*, 15(4): 381–88.